Microwave and Mechanical Considerations in the Design of MEM Switches for Aerospace Applications

Héctor J. De Los Santos, Yu-Hua Kao, Arturo L. Caigoy, and Eric D. Ditmars
Hughes Space and Communications Company
P.O. Box 92919, Bldg. S12, MS W327
Los Angeles, CA 90009-2919
310-416-4919
hjdelossantos@ccgate.hac.com

Abstract—Microelectromechanical Systems (MEMS) technology is expected to have tremendous impact on aerospace systems. Indeed, phased array antennas, frequency multiplexers, spacecraft GN&C, on-board communications, autonomous health monitoring & safety, space structures, thermal control, and on-board system reconfigurability will all be favorably and decisively impacted by MEMS technology. One of the most fundamental and ubiquitous components in these functions, enabled by MEMS technology, will be the electrostatic microelectromechanical (MEM) switch. The MEM switch, due to its simplicity and high performance potential, is poised to become the pioneering MEMS component, particularly, for microwave signal processing-related applications in space-based communications systems. This paper will discuss the impact of microwave performance specifications of the MEM switch on its mechanical structure and design. In particular, a *quantitative* discussion of switch parameters including actuation voltage, actuation frequency, insertion loss, and isolation will be presented.

TABLE OF CONTENTS

1. INTRODUCTION

Microelectromechanical Systems (MEMS) technology has received increasing attention from both industry and government agencies, who look at it as an enabler of weight, power consumption, and cost reductions. Microelectromechanical systems have great potential for many applications such as mechanical, optical, and fluidic systems, and batch fabrication methods germane to integrated circuit manufacturing. These systems can achieve tremendous efficiency and economies of scale[1], [2].

When compared to their macroscopic counterparts, the following advantages of MEMS have been identified: they are inherently smaller, lighter, faster, and possibly more precise [3]. The fundamental building blocks of many systems consist of three basic functions: sensing, decision making, and actuation. While the role of

0-7803-3741-7/97/$5.00

actuation is a critical part of most systems, the greater degree of mechanical complexity of the actuator elements, together with the additional issues of wear and friction, made its development lag that of microsensor capabilities [4]. Examples of mature MEMS components include accelerometers (used for triggering air bags in automobiles), pressure sensors (used in medical instrumentation), and nozzles (for ink jet and fuel injection). Other emerging components are gyroscopes, mechanical resonators, flow sensors, micropumps, microvalves, microactuators, microtweezers, torsional mirrors, switches, and micromotors [1]-[5]. The implementation of these systems exploits a variety of actuation mechanisms, namely, electrostatic, electromagnetic, magnetic, piezoelectric, shape memory alloy (SMA), thermoelectromechanical systems, etc. The mechanism of electrostatic actuation is particularly important with regards to surface micromachining processes. In particular, electrostatically-based actuators are most easily fabricated by the batch methods of IC-type processes, while also being most easily integrated with IC control [4].

Because of their simplicity, the most common and the most basic electrostatically-actuated surface-micromachined MEMS are the cantilever and the doubly-supported beams [6], Figure 1.

(a)

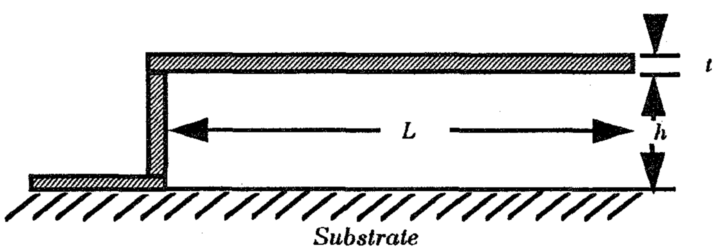

(b)

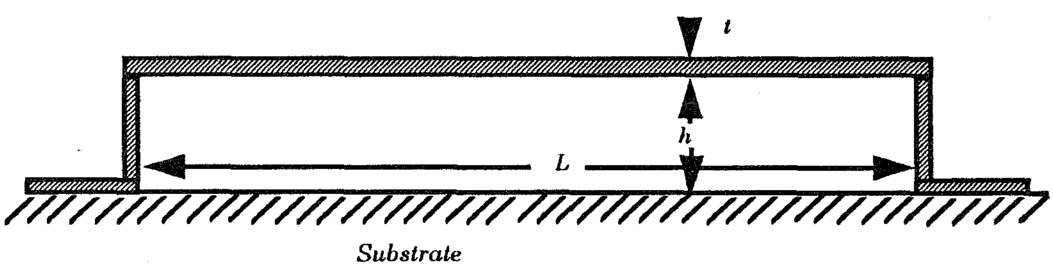

Figure 1. Schematic of typical surface-micromachined beams (a) cantilever beam-type, (b) doubly-supported beam.

An early cantilever beam-type MEM *switch* was first developed by Petersen [7], in the form of a cantilever beam composed of a thin (0.35μm), metal-coated insulating membrane attached to a silicon substrate at one end and suspended over a shallow rectangular pit. When a voltage was applied between the p+ silicon in the bottom of the pit and the deflection electrode metallization on the membrane surface, the cantilever beam experienced an electrostatic force of attraction distributed along its length, which pulled it downward until the membrane projection at the membrane tip made electrical contact with the fixed electrode. It became immediately apparent that these switches possessed nearly ideal electrical characteristics which made them suitable for applications requiring, for example, extremely high off-state to on-state impedance ratios, low off-state coupling capacitance, and very low switching and sustaining power.

Recently, the MEM switch has received renewed attention for application in integrated systems [8]-[11]. In one approach ([7], [8]), the switch consists of a deformable cantilever beam that realizes a segment of a signal-carrying microstrip transmission line, Figure 2a. With no actuation voltage applied, the beam is undeflected, so the line is open. With actuation voltage applied, the beam deflects, thus closing the gap while providing a continuous path through the transmission line. In a second approach [10], a cantilever beam is also used to make or break the path through a transmission line. In this case, however, the beam is perpendicular to the transmission line whose continuity the deflected beam is to either enable of disable, Figure 2b. Finally, in a third approach, a doubly-supported beam/membrane is used, Figure 2c. One segment of the signal-carrying transmission line originates on the substrate, right under the beam, while the other is part of the beam. Upon deflection of the beam the gap underneath it is closed, thus enabling continuity of the two line segments. Due to the excellent preliminary performance obtained with this type of switch, we will focus on the microwave and mechanical considerations in the design of cantilever beam-type MEM switches of the type that realizes a transmission line segment, Figure 2a.

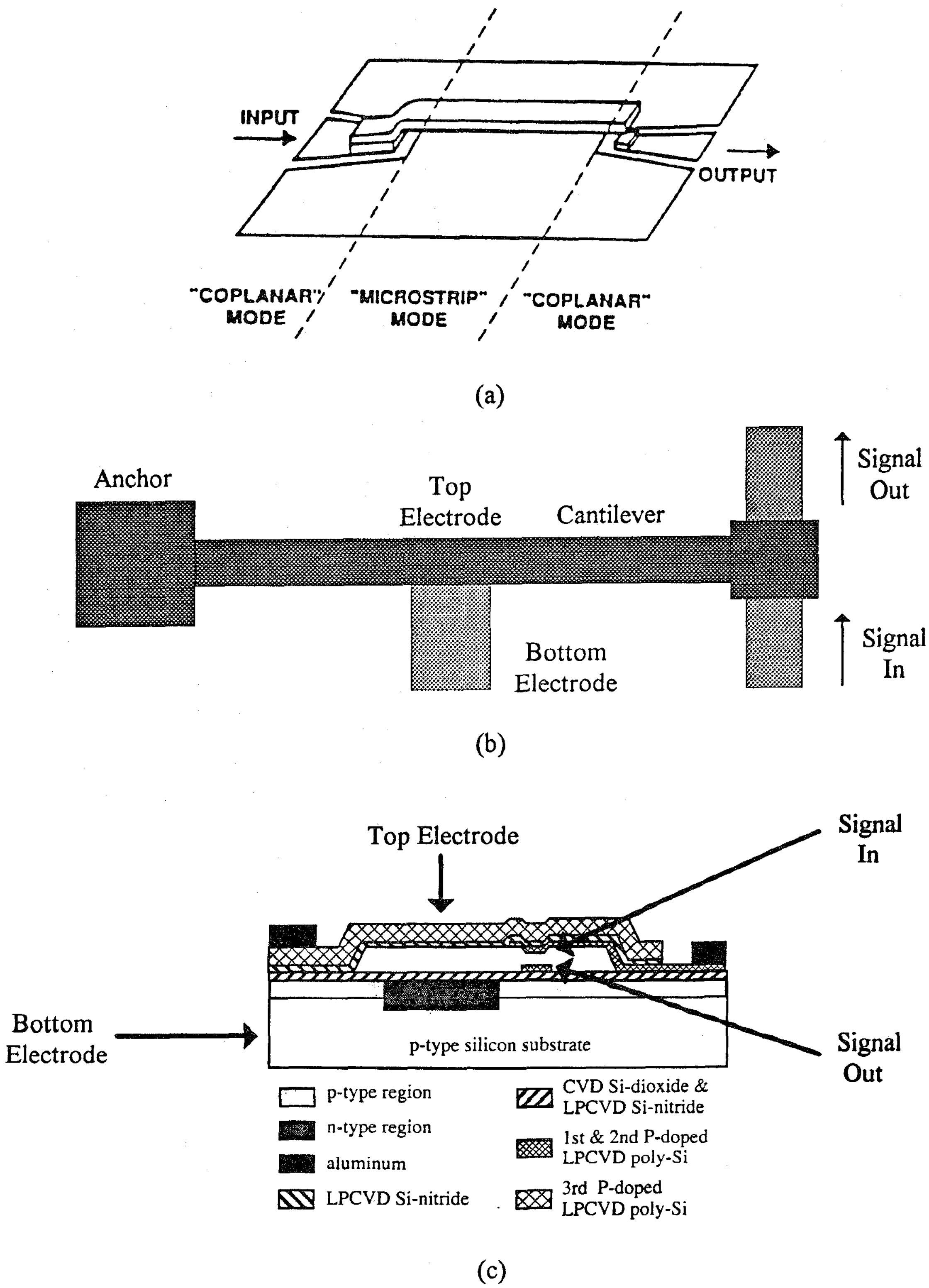

Figure 2. (a) Transmission line cantilever beam switch [8], (b) Orthogonal to signal line cantilever beam switch [11], (c) doubly-supported cantilever beam switch [9].

With no actuation voltage applied, the beam is undeflected, so the line is open. With actuation voltage applied, the beam deflects, thus closing the gap while providing a continuous path through the transmission line. In a second approach [10], a cantilever beam is also used to make or break the path through a transmission line. In this case, however, the beam is perpendicular to the transmission line whose continuity the deflected beam is to either enable or disable, Figure 2b. Finally, in a third approach, a doubly-supported beam/membrane is used, Figure 2c. One segment of the signal-carrying transmission line originates on the substrate, right under the beam, while the other is part of the beam. Upon deflection of the beam the gap underneath it is closed, thus enabling continuity of the two line segments. Due to the excellent preliminary performance obtained with cantilever beam-type MEM switches, Figure 2a, we will focus on its microwave and mechanical design considerations.

2. MEM SWITCH DESIGN CONSIDERATIONS

Switch Specifications

Ideally switches are components whose job it is to turn RF power on or off [12], or to perform high-frequency signal routing [13]. It is desirable for a switch to be *noninvasive* with respect to circuit/system performance. The degree of noninvasiveness exhibited by a switch is given by its electrical parameters [13]:

(1) Transition Time- is the time required for the RF voltage envelope to go from 10 percent to 90 percent for on-time, or 90 percent to 10 percent for off-time. At the 90 percent point, the signal is within 1 dB of its final value.

(2) Switching Speed- is the time required for the switch to respond at the output when the control line input voltage changes. Switching speed includes the driver propagation delay as well as transition time and is measured from the 50 percent point on the control voltage to 90 percent (for the on-time) or 10 percent (for the off-time) of the RF voltage envelope. Therefore, by definition, switching time will always be longer than transition time.

(3) Switching Transients- also called video leakage or video feedthrough, are exponentially decaying voltage spikes at the input and/or output of an RF switch that result when the control voltage changes. When observed on an oscilloscope, transients are measured as the peak deviation from a steady state baseline reference.

(4) RF Power Handling- this is a measure of how much and, in some respects, how well a switch passes the RF signal. To quantify RF power handling, the 1dB compression point is commonly specified. The 1dB compression point is a measure of the deviation from linearity of the 1dB output power with respect to the input power. In switches containing PN-junctions, e.g., PIN diodes and MMIC switches, power handling is a function of frequency.

(5) Intercept Point- is the extrapolation of the distortion power to the power level of the drive signals, assuming

the switch has no compression of the signals. It gives a useful number from which distortion at any drive power level may be computed.

(6) RF Insertion Loss and Isolation- are the loss a signal suffers upon traversing the switch, and the signal leakage appearing at the output when the switch is off, respectively.

In addition to the above parameters, the actuation voltage, the voltage necessary to effect switching, is an important switch parameter. The following MEM switch design considerations will be based on the schematic drawing shown in Figure 3.

Microwave Considerations

The structure of the cantilever beam switch must be chosen so as to produce the lowest possible insertion loss, the highest possible isolation, the highest possible switching frequency, and the lowest possible actuation voltage. The insertion loss will be affected by mismatch loss, which comes from the beam's characteristic impedance being different from 50 ohms (the normally used reference characteristic impedance), as well as losses in the beam metallization and contact resistance loss. The isolation, on the other hand, will be affected by the beam-to-substrate separation which defines the off-parasitic capacitance. Due to the inverse relation between beam-to-substrate separation and material stiffness, the low off-parasitic capacitance requirement is in conflict with low actuation voltage and high switching speed (resonance frequency) requirement. The electrical design of the switch, therefore, must be carried out in a self-consistent fashion with the mechanical/material design.

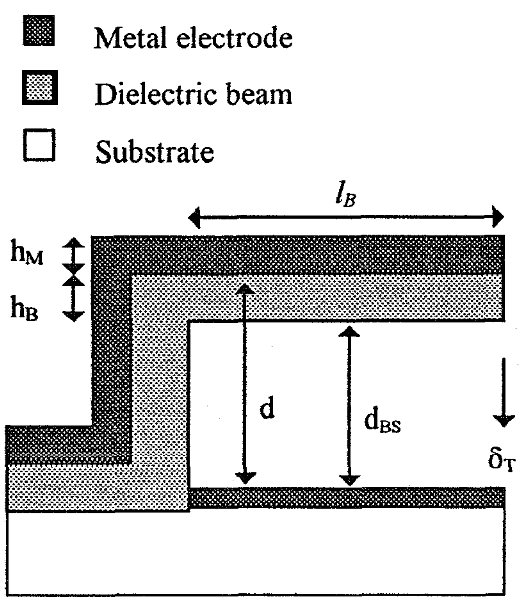

Parameters

l_B = Beam length
b_B = Beam width
h_B = Beam height
h_M = Top electrode thickness
d_{BS} = Beam-to-substrate distance
d = Electrode separation
$E_{B(M)}$ = Elastic modulus of beam (metal)
$\varepsilon_{r,B}$ = Relative dielectric constant of beam
$\varepsilon_{r,eff}$ = Effective relative dielectric constant of gap between electrodes
δ_T = Distance deflected at beam tip
$\rho_{B(M)}$ = Beam (metal) material density

Figure 3. Schematic of metal-coated cantilever beam used in deflection calculations.

For the electrical design of the MEM switch in Figure 2a, we consider it to be made up of a segment of a microstrip transmission line, Figure 4. Microstrip is used as interconnection media amongst devices in microwave circuits and systems where discrete devices comprising a circuit are bonded to a substrate. As the microstrip links the output of one device/circuit with the input of another, maximum power transfer considerations between circuits dictate that the microstrip's impedance, i.e., its *characteristic* impedance, Z_o, be set to a specific value. Through extensive electromagnetic analyses and curve fittings [14], a set of equations shown in Eqs. 1-20 have been obtained, whose iterative solution gives the desired characteristic impedance as a function of conductor width, w, substrate thickness, t_s, normalized conductor thickness, $t=t_s/(w/h)$, and substrate dielectric, ε_r. The iteration starts by obtaining an approximate value for the ratio u=w/h from Eqs. 1 and 2, which neglects the conductor thickness. Depending on whether the strip is embedded in a homogeneous media or in a mixed media, the ratio, u, is corrected by adding the terms Δu_a or Δu_r, respectively, as given in Eqs. 3 - 6. The characteristic impedance for a microstrip in a homogeneous medium, Z_{oa}, is obtained from Eqs. 7 and 8. The intrinsic wave impedance, η, is given by $\eta = \sqrt{\mu / \varepsilon_r}$, where μ and ε_r are the permeability and the permittivity of the substrate material, respectively. The corresponding characteristic impedance, Z_o, and effective dielectric constant, ε_{eff}, of the strip in the mixed medium, Figure 4, are obtained from Eqs. 9 - 13. Since u increases when Z_o decreases and vice versa, one very simple and effective method for finding the new approximation for w/h is by using the ratio in Eq. 14. Once convergence is achieved, the conduction losses are obtained from Eqs. 15 - 20. The skin-effect resistance of the conductor, given by R_m, is a function of the angular frequency, ω, the permeability of the substrate, μ, and the microstrip conductivity, σ.

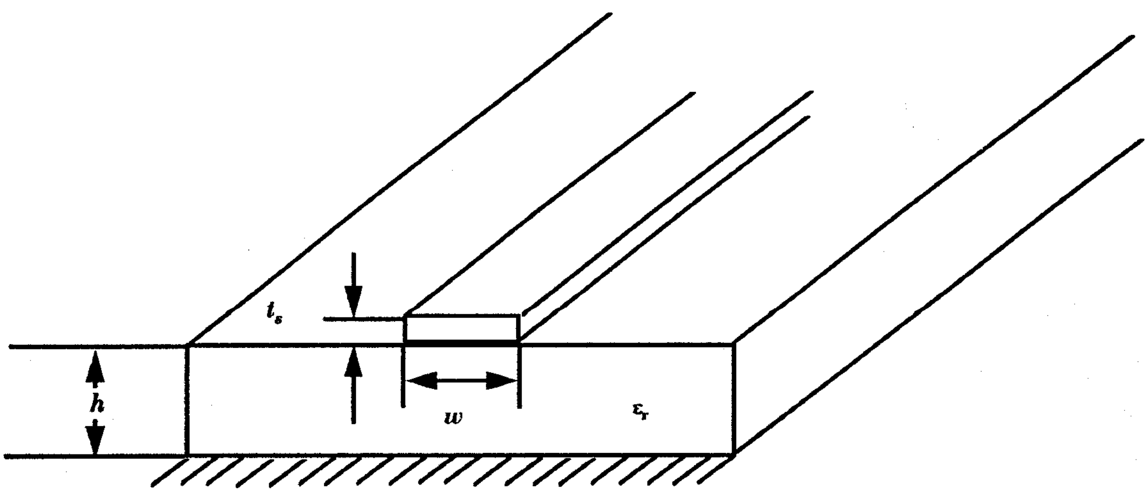

Figure 4. Microstrip transmission line.

$$\frac{w}{h} = 8\frac{\sqrt{\frac{A}{11}(7+4/\varepsilon_r)+\frac{1}{0.81}(1+1/\varepsilon_r)}}{A} \quad (1)$$

$$A = \exp\left(\frac{Z_0\sqrt{\varepsilon_r+1}}{42.4}\right) - 1 \quad (2)$$

$$\Delta u_a = \frac{t}{\pi}\ln\left[1+\frac{4\exp(1)}{t\cosh^2\sqrt{6.517w/h}}\right] \quad (3)$$

$$\Delta u_r = 1/2\left[1+1/\cosh\sqrt{\varepsilon_r-1}\right]\Delta u_a \quad (4)$$

$$u_a = \frac{w}{h} + \Delta u_a \quad (5)$$

$$u_r = \frac{w}{h} + \Delta u_r \quad (6)$$

$$Z_{0a}(u) = \frac{\eta}{2\pi}\ln\left[\frac{f(u)}{u}+\sqrt{1+\left(\frac{2}{u}\right)^2}\right] \quad (7)$$

$$f(u) = 6+(2\pi-6)\exp\left[-(\frac{30.666}{u})^{0.7538}\right] \quad (8)$$

$$\varepsilon_e(u,\varepsilon_r) = \frac{\varepsilon_r+1}{2}+\frac{\varepsilon_r-1}{2}\left(1+\frac{10}{u}\right)^{-s(u)b(\varepsilon_r)} \quad (9)$$

$$a(u) = 1+\frac{1}{49}\ln\left[\frac{u^4+\left(\frac{u}{52}\right)^2}{u^4+0.432}\right]+\frac{1}{18.7}\ln\left[1+\left(\frac{u}{18.1}\right)^3\right] \quad (10)$$

$$b(\varepsilon_r) = 0.564\left[\frac{\varepsilon_r-0.9}{\varepsilon_r+3}\right]^{0.053} \quad (11)$$

$$Z_0(w/h,t,\varepsilon_r) = Z_{0a}(u_r)\frac{Z_{0a}(u_r)}{\sqrt{\varepsilon_e(u_r,\varepsilon_r)}} \tag{12}$$

$$\varepsilon_{eff}(w/h,t,\varepsilon_r) = \varepsilon_f(u_r,\varepsilon_r)\left[\frac{Z_{0a}(u_a)}{Z_{0a}(u_r)}\right]^2 \tag{13}$$

$$\left(\frac{w}{h}\right)_{i+1} = \left(\frac{w}{h}\right)_i \frac{Z_0(w/h,t,\varepsilon_r)}{Z_0^{desired}} \tag{14}$$

$$\alpha_c = \left\{0.159A\frac{R_m\left[32-u_r^2\right]}{hZ_0\left[32+u_r^2\right]}; w/h \le 1\right. \tag{15}$$

$$\alpha_c = \left\{7.02\cdot 10^{-6}A\frac{R_m Z_0 \varepsilon_{eff}}{h}\left[u_r + \frac{0.667u_r}{u_r+1.444}\right]; w/h \ge 1\right. \tag{16}$$

$$A = 1 + u_r\left[1 + \frac{1}{\pi}\ln(2B/t)\right] \tag{19}$$

$$B_{\ge} = \left\{h; w/h \ge \pi/2\right. \tag{18}$$

$$B_{\le} = \left\{2\pi w; w/h \le \pi/2\right. \tag{19}$$

$$R_m = \sqrt{\frac{\omega\mu}{2\sigma}} \tag{20}$$

For the electromechanical design of the MEM switch, Figure 3 shows a schematic of the simple, metal-coated cantilever beam, along with the parameters involved in the electrostatically-actuated deflection calculations. Expressions for the threshold voltage for spontaneous beam deflection, V, the first transverse (bending) resonance frequency, f_R, and the maximum safe deflectable distance, x_{max}, are shown in Eqs. 21-23 [15-18].

As voltage is applied, a value is reached whereby the electrostatic force at the beam tip causes the beam to become unstable, resulting in spontaneous deflection of the remaining distance until actuation. The maximum deflectable distance is the maximum distance the beam can deflect prior to failure. Failure can be designated as the maximum allowable stress, σ_{max}, that exceeds the material yield strength, σ_y. Beyond this, elastic deformation ceases, and the material fails either catastrophically (ceramic and glasses) or plastically (metals). The maximum deflectable distance must at least exceed the beam-to-substrate distance traversed by the beam.

$$V = \sqrt{\frac{2(EI)_{eff} d_{BS}^{3} L}{\varepsilon_o \varepsilon_{r,eff} b_B l_B^{4}}} \tag{21}$$

$$f_R = \frac{0.162 h_B}{l_B^{2}} \sqrt{\frac{E_B K}{\rho_B}} \tag{22}$$

$$x_{\max} = \frac{l_B^{2} \sigma_{\max}}{3 E_{eff} h'} \tag{23}$$

Expressions for the terms appearing in Eqs. 21-23 are shown in Eqs. 24-32. The $(EI)_{eff}$ term is the product of the elastic modulus, E, and the moment of inertia, I, for the equivalent beam made up of more than one material, such as the metal-coated dielectric cantilever beam. The relative contribution of the metal and the dielectric to the mechanical properties of the equivalent beam is accounted for via the expressions for K', K", and K. The electrostatic load is integrated down the beam length, and the normalized load, L, required to produce a deflection is expressed in terms of a normalized deflection at the beam tip, Δ. To evaluate the influence of the dielectric constant on switching voltage, a $\varepsilon_{r,eff}$ term, derived from capacitors in series, is introduced as the effective dielectric constant of the dielectric beam and the void between the electrodes. However, for the case of a metal-only beam, instead of a composite beam, $\varepsilon_{r,eff}$ reduces to $\varepsilon_{r,air} = 1$, and E_{eff} simplifies to E_B.

$$(EI)_{eff} = \left(\frac{b_B h_B^{3}}{12}\right) \frac{h_M E_B E_M}{h_M E_M + h_B E_B} K' \tag{24}$$

$$K' = 4 + 6\left(\frac{h_M}{h_B}\right) + \left(\frac{E_B}{E_M}\right)\left(\frac{h_B}{h_M}\right) + 4\left(\frac{h_M}{h_B}\right)^{2} + \left(\frac{E_M}{E_B}\right)\left(\frac{h_M}{h_B}\right)^{3} \tag{25}$$

$$E_{eff} = \frac{(EI)_{eff}}{I_{eff}} = \frac{12(EI)_{eff}}{b_B (h_B + h_M)^{3}} \tag{26}$$

$$L = 4\Delta^2 \left[\frac{2}{3(1-\Delta)} - \frac{\tanh^{-1}\sqrt{\Delta}}{\sqrt{\Delta}} - \frac{\ln(1-\Delta)}{3\Delta} \right]^{-1} \quad (27)$$

$$\Delta = \frac{\delta_T}{d} \quad (28)$$

$$\frac{1}{\varepsilon_{r,eff}} = \frac{1}{d}\left(d_{BS} + \frac{h_B}{\varepsilon_{r,B}} \right) \quad (29)$$

$$K = K'K'' \quad (30)$$

$$K'' = \left(1 + \frac{E_B h_B}{E_M h_M} \right)\left(1 + \frac{\rho_M h_M}{\rho_B h_B} \right)^{-1} \quad (31)$$

$$h' = \frac{h_B + h_M}{2} \quad (32)$$

Material Considerations

The material parameters that determine the threshold voltage, the resonance frequency, and the maximum deflectable distance are the elastic modulus, the yield strength, and the dielectric constant. Table 1 lists these properties for different classes of materials.

Table 1. Elastic moduli, yield strengths, and dielectric constants of various materials [16, 19-27].

Class	Material	Elastic Modulus E (N/m^2)	Yield Strength σ_y (N/m^2)	Dielectric Constant, ε_r
Ceramics	Ta_2O_5	6.0×10^{10} (3)	---	25 (1)
	SiO_2	7.17×10^{10} (4)	8.4×10^{9} (6)	3.94 (1)
	Si_3N_4	1.3×10^{11} (1)	1.4×10^{10} (4)	7 (1)
	Al_2O_3	5.3×10^{11} (4)	1.54×10^{10} (4)	10 (1)
	TiO_2	5.95×10^{11} (4)	---	73 (2)
Metals	Au	6.13×10^{10} (5)	3.24×10^{8} (5)	---
	Al	7×10^{10} (4)	1.7×10^{8} (4)	---
	Cr	1.8×10^{11} (1)	3.62×10^{8} (4)	---
	Ni	2.07×10^{11} (4)	5.9×10^{7} (4)	---
Semiconductor	Si	1.90×10^{11} (7)	7.0×10^{9} (7)	13.5 (4)
Diamond	C	1.04×10^{12} (7)	5.3×10^{10} (7)	5.68 (4)

(1). Sputtered film (various temperatures), (2). MOCVD film (500°C), (3). Electron-beam evaporated film, (4). Bulk, (5). Vacuum-evaporated polycrystalline film (300°C), (6). Fiber, (7). Single crystal

The values of the mechanical and electrical properties of materials depend strongly on microstructure, such as whether the material is single crystal, polycrystal (grain size, grain orientation), amorphous, as-deposited, or annealed [27]. These process-sensitive material properties depend on the technology and the process parameters used in the construction of the MEM switch.

Using the data shown in Table 1, calculations based on Eqs. 21-32 reveal significant effects of material elastic modulus on switch performance, in terms of actuation voltage and frequency. For the two sets of switch dimensions shown in Table 2, Figure 5 shows that Au, Ta_2O_5, and SiO_2 require the lowest threshold voltages, and TiO_2 and diamond require the highest threshold voltages. As E increases, V increases. The dielectric constant does not correlate well with voltage. Higher voltage is required to switch a larger elastic modulus beam material, even though the dielectric constant is higher (e.g., compare Si and SiO_2 for their ε_r, E and required V). Thus, the dielectric constant plays a minor role but can become more influential at larger beam thicknesses.

Table 2. Threshold voltages for two sets of beam dimensions#.

Switch Dimensions :	1	2
Beam length l_B (μm)	106	(same)*
Beam width b_B (μm)	80	25
Beam height h_B (μm)	0.5	(same)
Beam-to-substrate d_{BS}(μm)	2	12

* Beam dimensions found in Ref. [28]. Results were reproduced.

Except for the Au beam, values are based on 50 nm-thick Au film as top electrode.

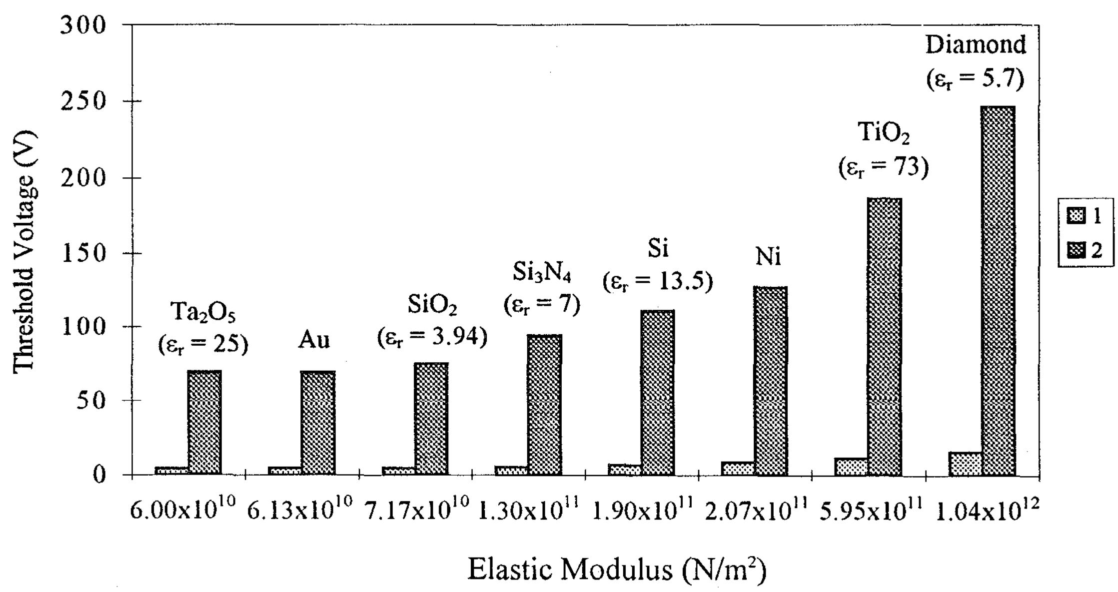

Figure 5. Effect of elastic modulus on threshold voltage for two sets of switch dimensions.

On the other hand, for each set of switch dimensions shown in Table 3, Figure 6 shows that Ta_2O_5, Au, and SiO_2 provide the *lowest* resonance frequencies. However, the stiffer materials, such as Si_3N_4, TiO_2 and diamond, will exhibit higher resonance frequencies. For the most part, with all else constant, the higher the E, the higher the f_R. (A beam made of Ni has lower resonant frequency because its density is significantly higher than the other materials with similar values of elastic modulus.)

Table 3. Resonant frequencies for three sets of beam dimensions*.

Switch Dimensions :	1	2	3
Beam length l_B (μm)	106	80	30
Beam width b_B (μm)	25	80	30
Beam height h_B (μm)	0.5	4.0	1.2
Beam-to-substrate d_{BS}(μm)	12	1	1

* Except for the Au beam, values are based on 50 nm-thick Au film as top electrode.

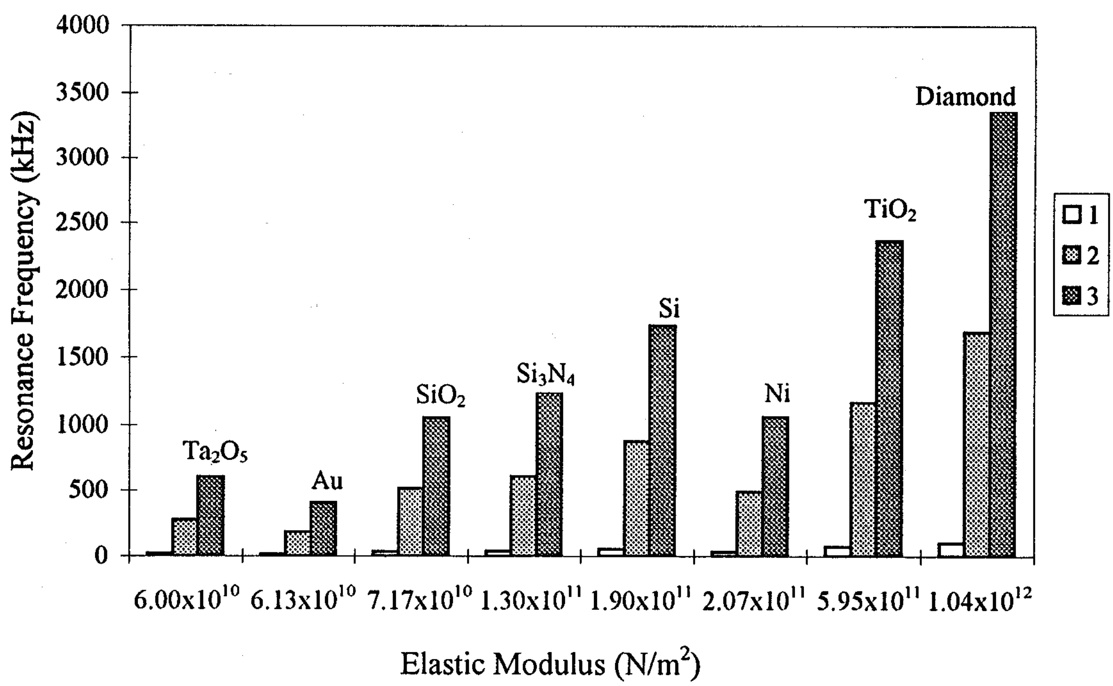

Figure 6. Effect of elastic modulus on resonant frequency for three sets of switch dimensions.

The elastic modulus was varied over several orders of magnitude to determine its effect on voltage (see Table 4 and Figure 7). Likewise, the dielectric constant was also varied over several orders of magnitude to determine its effect on voltage (see Table 5 and Figure 8). With all else constant, decreases in E cause significant drops in V. However, increases in ε_r do not cause appreciable decrease in V, although there is a small reduction. Thus, voltage is much more sensitive to elastic modulus than to dielectric constant. The gain in reducing the voltage by selecting a higher dielectric constant material is not as great as selecting a lower elastic modulus material.

Table 4. Reduction in threshold voltage by reducing elastic modulus for three sets of beam dimensions*.

Switch Dimensions :	1	2	3
Beam length l_B (μm)	106	(same)	(same)
Beam width b_B (μm)	25	(same)	(same)
Beam height h_B (μm)	2.0	0.5	1
Beam-to-substrate d_{BS}(μm)	2	12	12

* Values based on SiO_2 beam with $\varepsilon_r = 3.94$, and a 50 nm-thick Au film as top electrode.

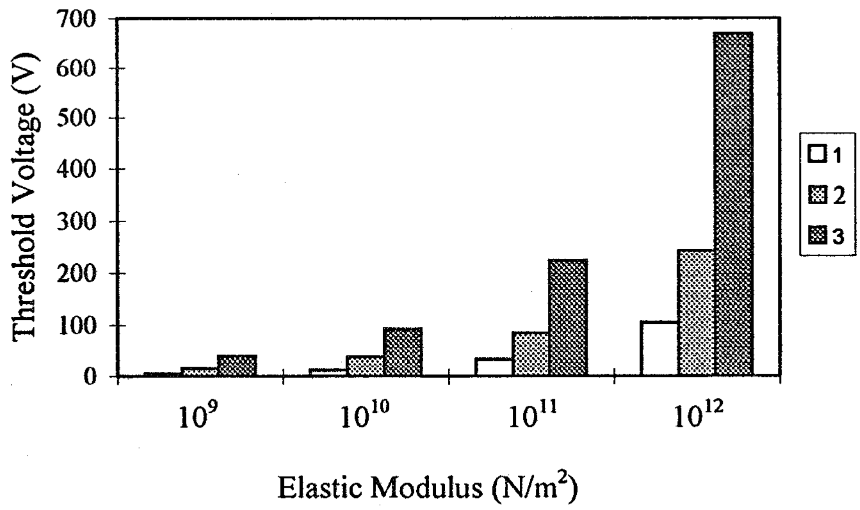

Figure 7. Effect of elastic modulus on threshold voltage for three sets of switch dimensions.

Table 5. Reduction in threshold voltage by increasing dielectric constant for three sets of beam dimensions*.

Dielectric Constant ε_r:	1	2	3
3.8	28.86	189.80	506.33
38	26.10	188.02	497.00
380	25.81	187.84	496.05
3,800	25.78	187.82	495.90
38,000	25.77	187.82	495.95
Switch Dimensions :			
Beam length l_B (μm)	106	(same)	(same)
Beam width b_B (μm)	25	(same)	(same)
Beam height h_B (μm)	2.0	1	2.0
Beam-to-substrate d_{BS}(μm)	2	12	12

* Values based on SiO_2 beam with $E = 7.17 \times 10^{10}$ N/m^2, and a 50 nm Au top electrode.

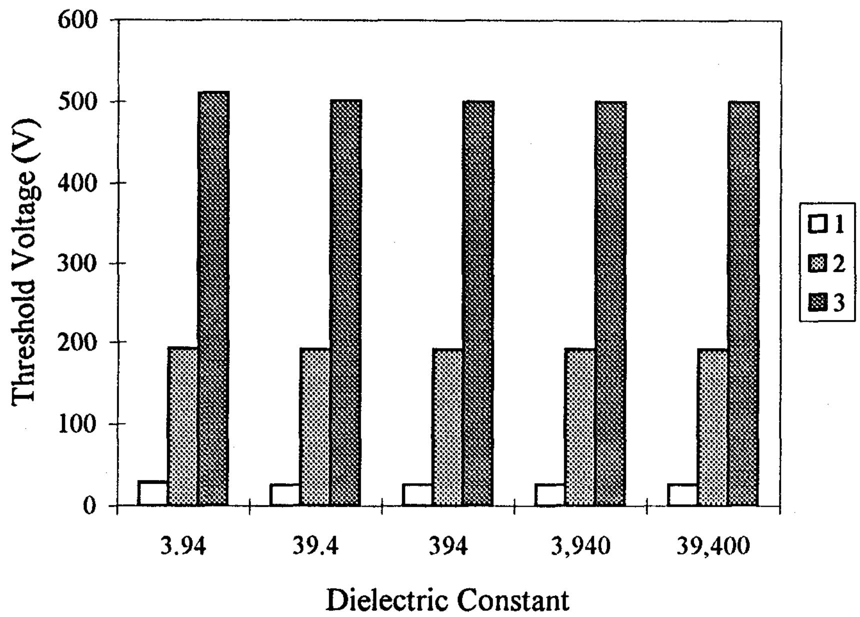

Figure 8. Effects of dielectric constant on voltage for three sets of switch dimensions.

In addition to these material considerations, fatigue reliability of the beam poses limitations on device lifetime. For long-life fatigue design, the switch must operate at some stress level sufficiently lower than the maximum expected stress. Measures of extending the fatigue life of the material can include eliminating surface defects/discontinuities such as grain boundaries, inclusions, and pores, which can be sources for crack-initiation, and reducing the beam strain (i.e., by minimizing the beam-to-substrate distance for actuation). Also, amorphous microstructures are preferred over polycrystalline microstructures for long-life fatigue cycling, since grain boundaries create stress concentrations for crack-initiated fatigue failures [29].

Mechanical Considerations

In addition to material considerations, device performance also depends on the optimization of switch dimensions. As Eqs. 21 and 22 show, a trade-off exists between voltage and resonance frequency for high device performance, such that low switching voltage also implies low switching speed. The dependencies of voltage and resonance frequency on switch dimensions are shown in Eqs. 33 and 34. Both voltage and resonance frequency depend inversely on beam length, l_B. However, voltage can be reduced independently by minimizing the beam-to-substrate distance, d_{BS}. (However, small beam-to-substrate distance leads to high off-parasitic capacitance.) The resonance frequency can be increased independently by increasing the beam thickness h_B. Two examples of switch dimensions that lead to switching speeds in the MHz regime while requiring relatively moderate (but not low) voltages are shown in Table 6.

$$V \propto \sqrt{\frac{d_{BS}^{3}}{b_B l_B^{4}}} \tag{33}$$

$$f_R \propto \frac{h_B}{l_B^{2}} \tag{34}$$

Table 6. Resonant frequencies and threshold voltages for two different sets of beam dimensions#.

Material :	f_{R1} (MHz)	V_1 (V)	f_{R2} (MHz)	V_2 (V)
Au	0.405	71	0.185	58
Ta_2O_5	0.594	49	0.275	28
SiO_2	1.041	59	0.513	40
Ni	1061	130	0.491	107
Si_3N_4	1.235	73	0.608	47
Si	1.723	85	0.877	52
TiO_2	2.361	143	1.167	82
Diamond	3.366	205	1.685	138
Switch Dimensions :				
Beam length l_B (μm)	30	30	80	80
Beam width b_B (μm)	30	30	80	80
Beam height h_B (μm)	1.2	1.2	4.0	4.0
Beam-to-substrate d_{BS}(μm)	1	1	1	1

Except for the Au beam, values are based on 50 nm-thick Au film as top electrode.

3. Discussion And Conclusions

In what follows, we present a summary of our findings using as vehicle actuation voltage, the insertion loss, the isolation, and the characteristic impedance for a MEM switch based on a Au-coated SiO_2 beam with a width of 50 μm and a length of 100 μm operating at 10 GHz. Figures 9 and 10 display our results.

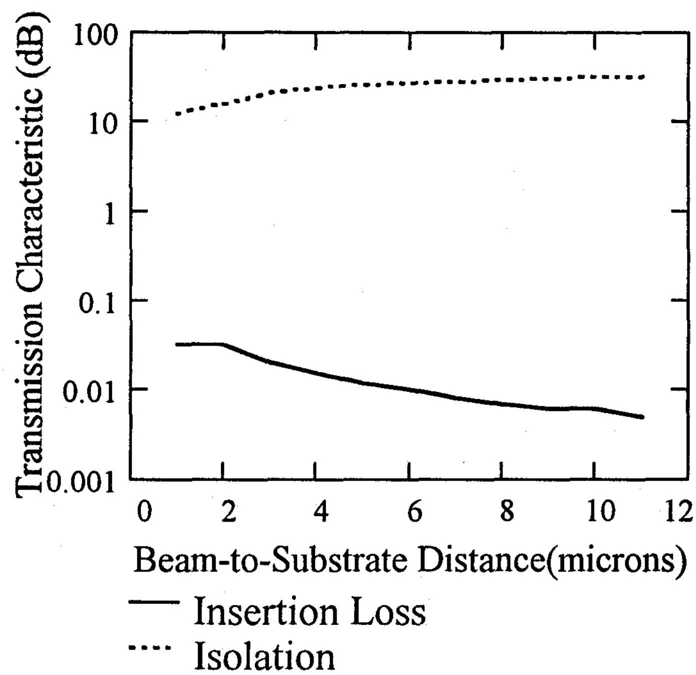

Figure 9. Insertion loss and isolation versus beam-to substrate distance. Frequency is 10 GHz.

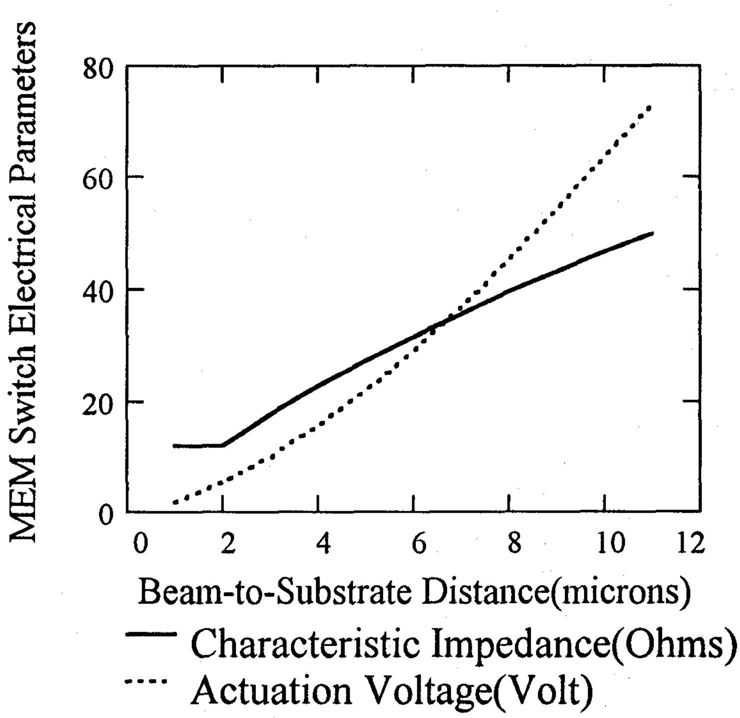

Figure 10. MEM switch characteristic impedance and actuation voltage versus beam-to-substrate distance. Frequency is 10 GHz.

As far as the electrical performance is concerned, Figures 9 and 10 clearly show that achieving a characteristic impedance close to 50 ohms demands a relatively large beam-to-substrate distance, and that this condition results in a large actuation voltage. On the other hand, a relatively high elastic modulus is necessary for applications requiring high frequency operation, but relatively low elastic modulus and small beam-to-substrate distance are necessary for applications requiring relatively low actuation voltages.

The switch design, therefore, will consist of a self-consistent iterative design/analysis cycle, until both the electrical and mechanical requirements are met. From the point of view of the electrical characteristics of the cantilever beam switch, the beam dimensions impact the device performance greatly, as opposed to, say, the material properties of the beam. However, important reliability considerations, germane to aerospace applications, will be determined by the material properties, in particular, the microstructure, the surface finish, and the residual stresses in the composite beam.

ACKNOWLEDGEMENT

The authors greatfully acknowledge the encouragement of Mr. Dorian Challoner and Mr. Burton Dobratz of Hughes Space and Communications Company.

REFERENCES

[1] W. Bacher, W. Menz and J. Mohr, "The LIGA Technique and Its Potential for Microsystems-A Survey," *IEEE Trans. Ind. Electronics* **42**, No. 5, pp. 431-441, October 1995.

[2] A.B. Frazier, R.O. Warrington and C. Friedrich, "The Miniaturization Technologies: Past, Present, and Future," *IEEE Trans. Ind. Electronics* **42**, No. 5 , pp. 423-431, October 1995.

[3] M. Mehregany, "An Overview of Microelectromechanical Systems," *Proc. SPIE* **1793**, Integrated Optics and Microstructures, pp. 2-11, 1992.

[4] J.J. Sniegowski and E.J. Garcia, "Microfabricated Actuators and Their Applications to Optics," *Proc. SPIE*, pp. 1-19, 1995.

[5] J. Bryzek, K. Petersen and W. McCulley, "Micromachines in the March, " *IEEE Spectrum*, pp. 20-31, May 1994.

[6] K.E. Petersen, "Microelectromechanical Membrane Switches on Silicon," *IBM J. Res. Develop.* **23**, No. 4, July 1979.

[7] Q. Meng, M. Mehregany and R.L. Mullen, "Theoretical Modeling of Microfabricated Beams with Elastically Restrained Supports," *J. Microelectromech. Syst* **2**, No. 3, pp. 128-137, September 1993.

[8] L.E. Larson, R.H. Hackett and R.F. Lohr, "Microactuators for GaAs-Based Microwave Integrated Circuits," *IEEE Transducers '91 Conference on Solid State Sensors and Actuators*, pp. 743-746, 1991.

[9] M.-A. Gretillat, P. Thiebaud, N.F. de Rooij and C. Linder, "Electrostatic Polysilicon Microrelays Integrated with MOSFETs," *1994 IEEE Micro Electro Mechanical Systems Workshop*, pp. 97-101, 1994.

[10] C. Goldsmith, T.-H. Lin, B. Powers, W.R. Wu, B. Norwell, "Micromechanical Membrane Switches for Microwave Applications,"*1995 IEEE MTT-S Digest*, pp. 91-94, 1995.

[11] J.J. Yao and M.F. Chang, "A Surface Micromachined Miniature Switch for Telecommunications Applications with Signal Frequencies from DC up to 4GHz", *8th Intl Conf. on Solid State Sensors and Actuators, and Eurosensors IX*, pp. 384-387, 1995.

[12] E. Blair, K. Farrington and K. Tubbs, "Selecting the Right RF Switch," *Microwave Journal*, June 1989.

[13] J. Browne, "Switches Perform High-Frequency Signal Routing," Microwaves & RF**??**, pp. 125-132, July 1989.

[14] W.A. Davis, *Microwave Semiconductor Circuit Design*, Van Nostrand Reinhold Company, Inc., pp. 126-128, 1984 ; H.A. Wheeler, "Transmission-Line Properties of a Strip on a Dielectric Sheet on a Plane," *IEEE Microwave Theory Tech.*, **MTT-25**, No. 8, pp. 631-647, August 1977 ; R.A. Pucel, D.J. Masse and C.P. Hartwig, "Losses in Microstrip," *IEEE Microwave Theory Tech.*, **MTT-16**, No. 6, pp. 342-350, June 1968 ; ____, "Corrections to 'Losses in Microstrip'," *IEEE Trans. Microwave Theory and Tech.*, **MTT-16**, p. 1064, December 1968 ; E. Hammerstad and O. Jensen, "Accurate Models for Microstrip Computer-Aided Design," *1980 IEEE MTT-S International Microwave Symposium Digest*, pp. 407-409, May 1980.

[15] K.E. Peterson, "Dynamic Micromechanics on Silicon: Techniques and Devices," *Transactions on Electron Devices* **ED-25**, No. 10, pp. 1241-1250, October 1978.

[16] K.E. Petersen and C.R. Guarnieri, "Young's Modulus Measurements of Thin Films Using Micromechanics," *Journal of. Applied Phys*ics **50**, No. 11, pp. 6761-6766, November 1979.

[17] R.J. Roark and W.C. Young, *Formulas for Stress and Strain*, 5th Ed., , New York: McGraw-Hill, pp. 112-113, 1956.

[18] R.L. Peek and H.N. Wagar, *Switching Relay Design*, New Jersey: Van Nostrand, pp. 32-35, 1995.

[19] K.E. Petersen, "Silicon as a Mechanical Material," *Proceedings of the IEEE* **70**, No. 5, pp. 4457, May 20, 1982.

[20] P.J. Martin, A. Bendavid, M.V. Swain, R.P. Netterfield, T.J. Kinder, W.G. Sainty and D. Drage, "Mechanical and Optical Properties of Thin films of Tantalum Oxide Deposited by Ion-Assisted Deposition," *Materials Research Society Symposium* **308**, pp. 583-588, 1993.

[21] W.D. Kingery, H.K. Bowen and D.R. Uhlmann, *Introduction to Ceramics*, 2nd Ed., New York: John Wiley & Sons, p. 933, 1976.

[22] C.A. Neugebauer, "Tensile Properties of Thin, Evaporated Gold Films," *Journal of Applied Physics* **31**, No. 6, June 1960.

[23] D. Benjamin, Ed., *Metals Handbook Ninth Edition*, Vol. 2 Properties and Selection: Nonferrous Alloys and Pure Metals, American Society for Metals, 1979.

[24] I.H. Pratt, "Thin Film Dielectric Properties of RF Sputtered Oxides," *Electronic Components Conference*, pp. 335-344, 1969.

[25] S.K. Tiku, "Choice of Dielectrics for TFEL Displays," *Transactions on Electron Devices*, **ED-31**, No. 1, pp. 105-108, January 1984.

[26] T.W. Kim, M Jung, H.J. Kim, T.H. Park, Y.S. Yoon, W.N. Kang, S.S. Yom and H.K. Na, "Optical and Electrical Properties of Titanium Dioxide Films with a High Magnitude Dielectric Constant Grown on p-Si by Metalorganic Chemical Vapor Deposition at Low Temperature," *Applied Physics Letters* **64**, No. 11, March 14, 1994.

[27] G.E. Dieter, *Mechanical Metallurgy*, 3rd Ed., New York: McGraw-Hill, 1986.

[28] K.E. Peterson, "Mechanical Light Modulator Array Fabricated on Silicon," *Applied. Physics Let*ters **31**, No. 8, pp. 376-382, October 15, 1977.

[29] H.O. Fuchs and R.I. Stephens, *Metal Fatigue in Engineering*, New York: John Wiley and Sons, 1980.

***Héctor J. De Los Santos** is a senior research engineer with the Advanced Electronics Operation of Hughes Space and Communications Company. He received a BSEE from the University of Puerto Rico, Mayagüez, an MSE from UCLA, and MS and PhD degrees in Solid State Devices and Materials from the School of Electrical Engineering, Purdue University. He is currently engaged in and directs research in the areas of High-Speed Monolithic Microwave Integrated Circuits, RF MEMS, Quantum Functional Devices, and Photonic Bandgap Materials and Applications.*

***Yu-Hua Kao** is a research engineer for the Thin Film Substrate Fabrication section of Hughes Space and Communications Company. She has a B.S. degree in Chemical Engineering from the University of Washington, and M.S. and Ph.D. degrees in Materials Science and Engineering from UCLA. Prior research area was in the development of*

nonlinear optical materials for photonic devices.

Eric D. Ditmars *is a manufacturing engineer/manager for Hughes Space and Communications (HSC) Company. He is the manager of the Thin Film Substrate Fabrication area for HSC. Previously, he was a Materials & Process engineer at McDonnell Douglas on the Space Station program. He has a B.S. degree in Materials Science and Engineering from MIT, and a M.S. degree in Material Science and Engineering from UCLA.*

Arturo L. Caigoy *is a research engineer for the Thin Film Substrate Fabrication section of Hughes Space and Communications Company. He is currently working on the development of new materials and technologies for microwave integrated circuits.*